Chapter 7

MERIDIONAL THROUGH-FLOW ANALYSIS

The term meridional through-flow analysis refers to an analysis of the flow in the meridional plane, i.e., a plane defined by a constant polar angle of cylindrical coordinates. A solution in the meridional plane can completely characterize the flow field if the flow is locally axisymmetric. This is usually considered to be a reasonable approximation for hub-to-shroud computing stations located outside of the blade rows. Hence, common practice is to locate all hub-to-shroud computing stations in a meridional through-flow analysis before, between or after the blade rows. This requires a means to define the influence of the blade rows in a form that can be imposed on the solution. Typically, this is accomplished by specifying the flow angle or swirl velocity and the entropy rise or total pressure loss associated with flow passing through the blade row. In the case of performance analysis of an existing axial-flow compressor design, the empirical models of Chapter 6 can be used. When designing an axial-flow compressor, the influence of the blade rows is specified directly. When the meridional through-flow analysis is completed, the geometry of the blade rows is selected to produce the specified influence.

A properly formulated meridional through-flow analysis is a very powerful technique that can be used to support a variety of axial-flow compressor aerodynamic design and analysis functions. In this book, this technique will be used for aerodynamic performance analysis, general stage design and complete axial-flow compressor design. This chapter develops the governing equations and describes methods of solution appropriate to these various applications.

NOMENCLATURE

A = annulus area
a = sound speed
B_{wake} = wake blockage
B^* = stream surface repositioning damping factor
C = absolute velocity
F = general function
f = general function

H = total enthalpy
h = static enthalpy
I = rothalpy
K_B = boundary layer blockage factor
K_W = wake blockage factor
M = Mach number
m = meridional coordinate
$\dot{m}$ = mass flow rate
n = normal coordinate
P = pressure
r = radius
s = entropy
T = temperature
W = relative velocity
y = coordinate along a quasi-normal
z = axial coordinate
β = flow angle with m-direction
ε = $\phi - \lambda$; deviation of quasi-normal from a true stream surface normal
κ_m = stream surface curvature
λ = quasi-normal angle, Eq. (7-1)
ϕ = stream surface angle with axial direction
θ = polar angle
ρ = gas density
ω = rotation speed (radians/second)

Subscripts

h = hub parameter
m = meridional component
s = shroud parameter
t = total thermodynamic condition
θ = tangential component
1 = condition at point preceding point being considered
2 = condition at point being considered
3 = condition at point following point being considered

Superscripts

$'$ = relative condition
$*$ = parameter on stream surface where W_m is specified for annulus sizing

7.1 Meridional Coordinate System

Figure 7-1 illustrates the basic meridional coordinate system used in a meridional through-flow analysis. A series of meridional computing stations or

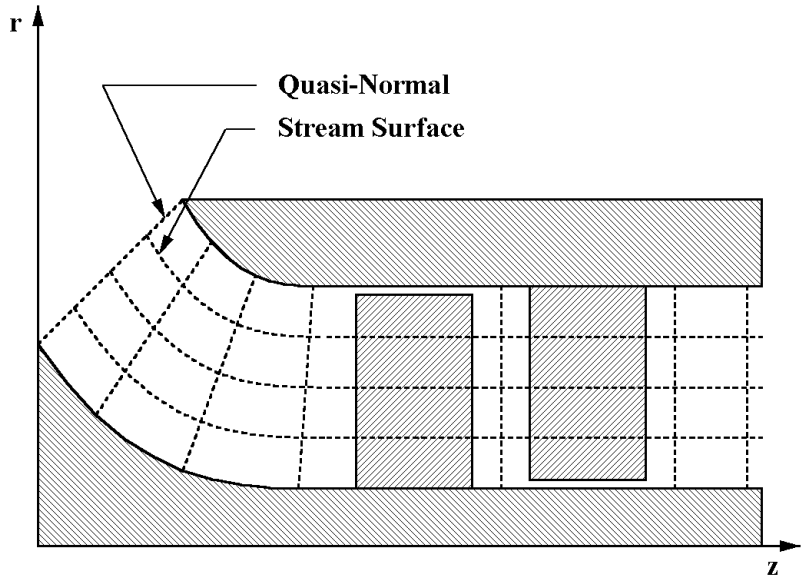

FIGURE 7-1 Definition of the Problem

straight-line quasi-normals are distributed through the compressor, all of which lie outside of the blade rows. The annulus is divided into a series of stream tubes separated by stream surfaces. A stream surface is defined as a surface having no mass flow across it, or equivalently, no velocity component normal to it. Hence, the hub and shroud contours always define stream surfaces. The intermediate stream surfaces are normally defined by requiring that the mass flow between each stream surface and the hub stream surface be constant through the solution domain. Quasi-normals in axial-flow compressors are often simple radial lines, although provision should be made for non-radial quasi-normals to treat cases such as that of the inlet section illustrated in Fig. 7-1.

Figure 7-2 illustrates the quasi-normal construction in further detail. As the name implies, the intention is to construct the quasi-normal to be approximately normal to the stream surfaces. The quasi-normal is defined by the (z, r) coordinates of both end points or by one end point plus the quasi-normal angle, λ. As illustrated in Fig. 7-2, the quasi-normal angle is defined by

$$\tan \lambda = \frac{\Delta z}{\Delta r} = \frac{z_h - z_s}{r_s - r_h} \tag{7-1}$$

The stream surface slope angle, ϕ, is given by

$$\sin \phi = \frac{\partial r}{\partial m} \tag{7-2}$$

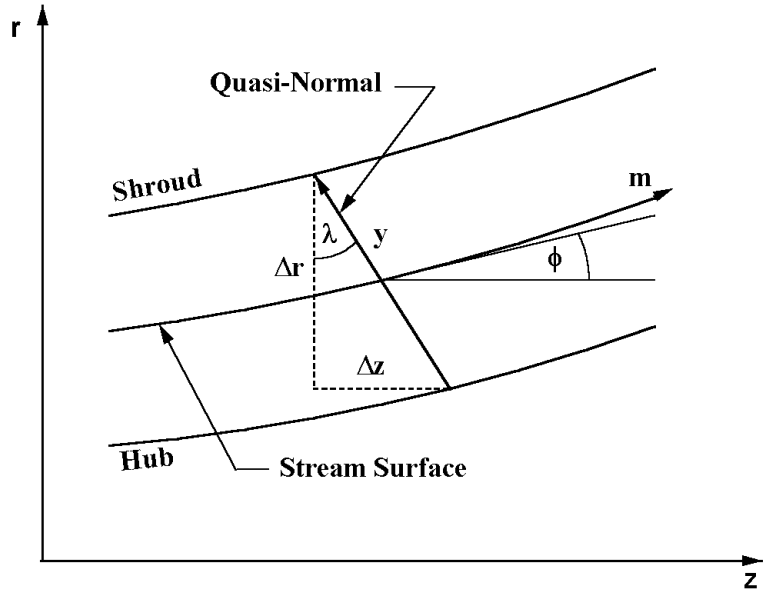

FIGURE 7-2 Quasi-Normal Construction

where m is the meridional coordinate, measured along a stream surface. Noting that λ is also the angle between a normal to the quasi-normal and the axial direction, the angle, ε, between a quasi-normal and a true stream-surface normal is given by

$$\varepsilon = \phi - \lambda \tag{7-3}$$

Quasi-normals do not have to be defined with extreme precision, but it is preferred that ε be relatively small if possible to achieve better numerical accuracy. This means that ε on the hub-and-shroud contours should be approximately equal in magnitude, but opposite in sign. In axial-flow compressors, this is usually not an important consideration since a simple radial quasi-normal normally results in very small values of ε. But for cases like that of the inlet passage illustrated in Fig. 7-1, a little more care may be needed.

In Chapter 3, the governing equations for adiabatic inviscid flow were developed in the natural coordinate system (θ, m, n). This coordinate system is convenient for derivation of the equations, but less convenient for solution. The reason is that two of the coordinates, m and n, must be determined as part of the solution. It is advantageous to maintain the stream surface coordinate, m, despite the need to compute it in the solution, since many of the basic conservation equations explicitly apply along m. But the determination of n is an unnecessary complication offering no benefit to a numerical analysis. Katsanis (1964) suggested the use

of the quasi-normal coordinate, y, shown in Fig. 7-2, to avoid that complication. It is easily shown that derivatives with respect to n can be expressed in the form

$$\frac{\partial}{\partial n} = \frac{1}{\cos\varepsilon}\left[\frac{\partial}{\partial y} - \sin\varepsilon\frac{\partial}{\partial m}\right] \tag{7-4}$$

Since y is a fixed coordinate at all computing stations, the numerical analysis is greatly simplified.

7.2 INVISCID ADIABATIC FLOW ON A QUASI-NORMAL

The relevant equations for adiabatic inviscid flow are developed in general form in Chapter 3. For the present application, Eqs. (3-21), (3-25), (3-29) and (3-30) can be used after they are simplified to their axisymmetric, time-steady form. It will be convenient to satisfy conservation of mass in integral form instead of using Eq. (3-21). Conservation of mass along a quasi-normal can be expressed in the form

$$\dot{m} = 2\pi K_B \int_0^{y_s} K_W r\rho W_m \cos\varepsilon\, dy \tag{7-5}$$

K_B is the end-wall boundary layer blockage factor, which corrects the area available for through-flow for viscous blockage effects. It is the fraction of the total area available for through-flow after subtracting the hub-and-shroud boundary layer displacement thicknesses from the overall quasi-normal length. Methods to estimate K_B will be described in Chapter 8. For now, it is simply recognized that it must be specified in some manner. K_W is the blade wake blockage factor, which serves a similar purpose in correcting for local wake blockage. From Eqs. (6-83) and (6-84), it is given by

$$K_W = 1 - B_{wake} \tag{7-6}$$

The axisymmetric, time-steady tangential and normal momentum equations follow directly from Eqs. (3-29) and (3-30).

$$\frac{\partial(rW_\theta + \omega r^2)}{\partial m} = \frac{\partial rC_\theta}{\partial m} = 0 \tag{7-7}$$

$$\kappa_m W_m^2 + \frac{W_\theta}{r}\frac{\partial(rW_\theta + \omega r^2)}{\partial n} + W_m\frac{\partial W_m}{\partial n} = \frac{\partial I}{\partial n} - T\frac{\partial s}{\partial n} \tag{7-8}$$

where κ_m is the stream surface curvature given by Eq. (3-26), i.e.,

$$\kappa_m = -\frac{\partial\phi}{\partial m} \tag{7-9}$$

The axisymmetric, time-steady energy equation follows directly from Eq. (3-25).

$$\frac{\partial I}{\partial m} = 0 \tag{7-10}$$

Substitution of Eqs. (7-7) and (7-10) into Eq. (3-28) shows that for axisymmetric flow, entropy must also be conserved in the meridional direction, i.e.,

$$\frac{\partial s}{\partial m} = 0 \tag{7-11}$$

At first glance, Eqs. (7-7) and (7-11) would appear to preclude use of this model for axial-flow compressors. It is known that entropy and angular momentum change along stream surfaces when the flow passes through blade rows. But these equations do not preclude changes between quasi-normals. They only require that the local gradients be zero for the flow to be locally axisymmetric. Introducing Eq. (7-4) into Eq. (7-8), and simplifying the result with Eqs. (7-7), (7-10) and (7-11), yields the following expression for the normal momentum equation.

$$W_m \frac{\partial W_m}{\partial y} + \kappa_m W_m^2 \cos\varepsilon - W_m \sin\varepsilon \frac{\partial W_m}{\partial m} + \frac{W_\theta}{r} \frac{\partial (rC_\theta)}{\partial y} = \frac{\partial I}{\partial y} - T \frac{\partial s}{\partial y} \tag{7-12}$$

Equation (7-12) can also be expressed in terms of the relative flow angle, noting that $W_\theta = W_m \tan\beta'$.

$$W_m \frac{\partial W_m}{\partial y} + \kappa_m W_m^2 \cos\varepsilon - W_m \sin\varepsilon \frac{\partial W_m}{\partial m} + \frac{W_m \tan\beta'}{r} \frac{\partial (rW_m \tan\beta' + \omega r^2)}{\partial y} = \frac{\partial I}{\partial y} - T \frac{\partial s}{\partial y} \tag{7-13}$$

After some basic algebra and trigonometry, Eq. (7-13) simplifies to the form

$$\frac{W_m}{\cos^2\beta'} \frac{\partial W_m}{\partial y} + \kappa_m W_m^2 \cos\varepsilon - W_m \sin\varepsilon \frac{\partial W_m}{\partial m} + \frac{W_m^2 \tan\beta'}{r} \frac{\partial (r\tan\beta')}{\partial y} + 2W_m \omega \tan\beta' \cos\lambda = \frac{\partial I}{\partial y} - T \frac{\partial s}{\partial y} \tag{7-14}$$

It is convenient to express the normal momentum equation in the following general form:

$$\frac{\partial W_m}{\partial y} = f_1(y) W_m + f_2(y) + \frac{f_3(y)}{W_m} \tag{7-15}$$

When C_θ and W_θ are known, the functions in Eq. (7-15) are

$$f_1(y) = -\kappa_m \cos\varepsilon + \frac{\sin\varepsilon}{W_m}\frac{\partial W_m}{\partial m} \tag{7-16}$$

$$f_2(y) = 0 \tag{7-17}$$

$$f_3(y) = \frac{\partial I}{\partial y} - T\frac{\partial s}{\partial y} - \frac{W_\theta}{r}\frac{\partial (rC_\theta)}{\partial y} \tag{7-18}$$

When β' is known, the functions are

$$f_1(y) = \cos^2\beta'\left[-\kappa_m \cos\varepsilon - \frac{\tan\beta'}{r}\frac{\partial (r\tan\beta')}{\partial y} + \frac{\sin\varepsilon}{W_m}\frac{\partial W_m}{\partial m}\right] \tag{7-19}$$

$$f_2(y) = -2\omega\cos\beta'\sin\beta'\cos\lambda \tag{7-20}$$

$$f_3(y) = \cos^2\beta'\left[\frac{\partial I}{\partial y} - T\frac{\partial s}{\partial y}\right] \tag{7-21}$$

Numerical integration of Eq. (7-15) is straightforward if the functions f_1, f_2 and f_3 are truly functions of y only. But it can be seen that f_3 includes a term involving the meridional gradient of W_m, which appears to depend on the flow solution on other quasi-normals. Novak (1967) shows that this difficulty can be removed by use of the differential form of the continuity equation, i.e., Eq. (3-21). For time-steady, axisymmetric flow, this reduces to

$$\frac{\partial (r\rho W_m)}{\partial m} + \kappa_n r\rho W_m = 0 \tag{7-22}$$

Combining Eqs. (3-27) and (7-21) and expanding the result yields

$$\frac{1}{W_m}\frac{\partial W_m}{\partial m} + \frac{1}{\rho}\frac{\partial \rho}{\partial m} + \frac{\sin\phi}{r} + \frac{\partial \phi}{\partial n} = 0 \tag{7-23}$$

Since entropy is conserved along stream surfaces, the term involving the gradient of ρ can be expanded using Eq. (2-26) to yield

$$\frac{1}{\rho}\frac{\partial \rho}{\partial m} = \frac{1}{\rho}\frac{\partial P}{\partial m}\left(\frac{\partial \rho}{\partial P}\right)_s = \frac{1}{\rho a^2}\frac{\partial P}{\partial m} \tag{7-24}$$

Finally, introducing Eq. (3-22) for time-steady axisymmetric flow yields

$$\frac{1}{\rho}\frac{\partial \rho}{\partial m} = \frac{1}{a^2}\left[\frac{C_\theta^2 \sin\phi}{r} - W_m\frac{\partial W_m}{\partial m}\right] \tag{7-25}$$

Combining Eqs. (7-23) and (7-25) yields

$$\frac{1}{W_m}\frac{\partial W_m}{\partial m}(1-M_m^2) = -(1+M_\theta^2)\frac{\sin\phi}{r} - \frac{\partial \phi}{\partial n} \tag{7-26}$$

where the meridional and tangential Mach numbers are given by

$$M_m = W_m / a \tag{7-27}$$

$$M_\theta = C_\theta / a \tag{7-28}$$

Introducing Eqs. (7-4) and (7-9) into Eq. (7-26) yields

$$\frac{1}{W_m}\frac{\partial W_m}{\partial m}(1-M_m^2) = -(1+M_\theta^2)\frac{\sin\phi}{r} - \frac{1}{\cos\varepsilon}\frac{\partial \phi}{\partial y} - \kappa_m \tan\varepsilon \tag{7-29}$$

Hence, Eq. (7-29) can be used to evaluate the meridional gradient of W_m on any quasi-normal, independent of the solution on other quasi-normals. It is necessary to take the precaution of avoiding a singularity only if $M_m = 1$ should occur. This writer imposes the following constraint when applying Eq. (7-29).

$$1 - M_m^2 \geq 0.1 \tag{7-30}$$

Equation (7-15) can also become singular if $W_m = 0$. Aungier (2000) avoids that problem by using conservation of mass in a stream tube in the form

$$\Delta \dot{m} = \rho W_m \Delta A \tag{7-31}$$

The stream tube area term is given by

$$\Delta A = 2\pi r K_W \cos\varepsilon \, \Delta y \tag{7-32}$$

Typically, all stream tubes are assumed to contain equal mass flows, although alternate definitions can certainly be used. Now introduce the function, f_4, given by

$$f_4(y) = f_2(y) + f_3(y)\frac{\rho \Delta A}{\Delta \dot{m}} \tag{7-33}$$

Then, Eq. (7-15) can be written as

$$\frac{\partial W_m}{\partial y} = f_1(y) W_m + f_4(y) \tag{7-34}$$

The solution of this linear differential equation can be found in almost any textbook on differential equations as

$$W_m(y) = W_m(0)F(y) + F(y)\int_0^y \frac{f_4(y)}{F(y)}dy \tag{7-35}$$

where the function $F(y)$ is given by

$$F(y) = \exp\left[\int_0^y f_1(y)dy\right] \tag{7-36}$$

The meridional velocity on the hub contour, $W_m(0)$, is the constant of integration for Eq. (7-34). It is determined from conservation of mass through Eq. (7-5). Equations (7-34) and (7-5) are solved in an iterative numerical scheme, successively improving the estimate of $W_m(0)$ until mass is conserved and the normal momentum equation is satisfied. This requires calculation of thermodynamic properties such as ρ and a, using an appropriate equation of state from Chapter 2. At any point, the relative total enthalpy is given by Eq. (3-13), i.e.,

$$H' = I + \tfrac{1}{2}(r\omega)^2 \tag{7-37}$$

The local static enthalpy is given by

$$h = H' - \tfrac{1}{2}W^2 \tag{7-38}$$

Then static thermodynamic conditions are computed from relative total thermodynamic conditions for the change in enthalpy, $(h - H')$, while holding entropy constant.

When computing the flow profile on a quasi-normal, it is also necessary that the numerical analysis be able to recognize choked flow. The choke condition corresponds to the maximum mass flow rate that can pass through the annulus for the specified total thermodynamic conditions and swirl velocity or flow angle. One way to identify choke is to compare mass flow rates calculated from Eq. (7-5) for two different values of $W_m(0)$. If the calculated mass flow and $W_m(0)$ vary in opposite directions, the higher value of $W_m(0)$ is beyond the choke limit. An iteration scheme can be used to converge on the actual choking value of $W_m(0)$. It has been found to be simpler, and equally effective, to monitor the average meridional Mach number, M_m, of Eq. (7-27). For uniform, swirling flow in an annulus, it can be shown that the condition for choke is $M_m = 1$. For the more general case considered here, a reasonable criterion for choke is

$$\frac{1}{y_s}\int_0^{y_s} M_m dy \geq 1 \tag{7-39}$$

Indeed, this parameter is easily employed to limit the value of $W_m(0)$ used while seeking to converge on the mass flow. The existence of a choke condition at

a quasi-normal is not necessarily an indication of choke for the compressor. It can be caused by incorrect stream sheet geometry in the early iterations. Hence, the overall numerical scheme must include provision to continue the analysis until it is clear that the choke condition is real. But during the process of calculating the flow profiles on a specific quasi-normal, it does represent the maximum mass flow rate that can pass through the annulus.

The procedure and equations outlined in this section can be used to compute the flow along a quasi-normal under the following conditions:

- The stream surface coordinates, slopes and curvatures along the quasi-normal are specified.
- The total thermodynamic conditions along the quasi-normal are specified.
- The flow angle or the swirl velocity distribution along the quasi-normal is specified.

What remains is description of how these conditions are to be established in the overall numerical analysis. For generality, the procedures described are presented for the rotating frame of reference. They are equally valid for the stationary frame of reference if $\omega = 0$ and C, β and H are substituted for W, β' and I, respectively.

7.3 LINKING QUASI-NORMALS

Next, the determination of the total thermodynamic conditions and swirl or flow angle profiles on a quasi-normal will be considered. It will continue to be assumed that the stream surface coordinates, slopes and curvatures are all known. This section describes techniques needed to link successive quasi-normals together so that the quasi-normal flow analysis of the previous section can be conducted on all quasi-normals for a specified stream surface pattern.

To start the process, boundary conditions are needed for the first quasi-normal. The usual process is to supply specifications of the distributions of the inlet flow angle or absolute tangential velocity and inlet total thermodynamic conditions (e.g., P_t and T_t) along the first quasi-normal. Values of these parameters on the stream surfaces of the first quasi-normal are determined by interpolation from these profile specifications. Then the procedures of the previous section can be used to compute the inlet flow profiles.

For all quasi-normals after the first one, the process required is to link the quasi-normal being analyzed to the upstream quasi-normal, where all flow data are known. Subscript 1 will be used to designate known data on the upstream quasi-normal, and subscript 2 will be used to designate conditions on the quasi-normal being analyzed, where both apply to the same stream surface. The simplest case is successive quasi-normals in a simple annular passage with no blade row between them. In this case, Eqs. (7-7), (7-10) and (7-11) provide the linking relations, i.e.,

$$(rC_\theta)_2 = (rC_\theta)_1 \tag{7-40}$$

$$I_2 = H_2 - \omega(rC_\theta)_2 = I_1 = H_1 - \omega(rC_\theta)_1 \tag{7-41}$$

$$s_2 = s_1 \tag{7-42}$$

From Eqs. (7-40) and (7-41), it is seen that $H_2 = H_1$ is the true linking condition implied by Eq. (7-41). Hence, all data needed for the quasi-normal flow analysis of the previous section are available.

When a blade row lies between the two quasi-normals, the empirical models of Chapter 6 are used to estimate the influence of the blade row. The process will be described in the rotating frame of reference, recognizing that it is applied to a stationary blade by simply setting $\omega = 0$. The empirical models of Chapter 6 supply the blade row total pressure loss coefficient and discharge relative flow angle. But the empirical models require knowledge of the discharge meridional velocity, which is not yet known. Hence, an iterative solution procedure is required, typically starting with the assumption that $W_{m2} = W_{m1}$ on all stream surfaces. The estimate of the discharge meridional velocity profile is improved by successive application of the empirical models of Chapter 6 and the quasi-normal flow analysis of the previous section until the process converges. First, the inlet relative conditions are computed from the known upstream absolute flow conditions.

$$I_1 = H_1 - \omega(rC_\theta)_1 \tag{7-43}$$

$$W_{\theta 1} = C_{\theta 1} - r_1\omega \tag{7-44}$$

$$W_1 = \sqrt{W_{m1}^2 + W_{\theta 1}^2} \tag{7-45}$$

$$H_1' = h_1 + \tfrac{1}{2}W_1^2 \tag{7-46}$$

Other relative total conditions (e.g., P'_{t1} and T'_{t1}) can be computed from the equation of state and the known values of entropy and relative total enthalpy. At the discharge station, conservation of rothalpy requires

$$I_2 = I_1 \tag{7-47}$$

$$H_2' = I_2 + \tfrac{1}{2}(r_2\omega)^2 \tag{7-48}$$

The ideal (no loss) discharge total pressure is computed from the equation of state, using the known discharge relative total enthalpy and the inlet entropy. Then the actual discharge relative total pressure is computed from the total pressure loss coefficient.

$$P'_{t2} = P'_{t2id} - \overline{\omega}(P'_{t1} - P_1) \tag{7-49}$$

All other relative total thermodynamic conditions and the entropy at the discharge are computed using the equation of state and the known relative total pressure and relative total enthalpy. Hence, all data required for the quasi-normal

flow analysis of the previous section are known. When the blade performance and discharge flow profile iteration process is converged, absolute discharge conditions are computed as

$$C_{\theta 2} = W_{\theta 2} + r_2\omega = W_{m2}\tan\beta_2' + r_2\omega \tag{7-50}$$

$$H_2 = I_2 + \omega(rC_\theta)_2 \tag{7-51}$$

$$C_{m2} = W_{m2} \tag{7-52}$$

$$C = \sqrt{C_{m2}^2 + C_{\theta 2}^2} \tag{7-53}$$

7.4 REPOSITIONING THE STREAM SURFACES

After solving the equations for conservation of mass and momentum to determine all flow field data throughout the solution domain, the new data will generally not be consistent with the stream surface geometry used in the process. The variation of mass flow along any quasi-normal can be easily determined in functional form using a modified form of Eq. (7-5).

$$\dot{m}(y) = 2\pi\int_0^y K_W r\rho W_m \cos\varepsilon\, dy \tag{7-54}$$

Note that the boundary layer blockage factor, K_B, has been omitted in Eq. (7-54). This writer prefers to treat the blockage factor as a simple area correction applied to conservation of mass. In this approach, the hub-and-shroud stream surfaces are always positioned on the corresponding end-wall contours. An alternate approach is to reposition the hub-and-shroud stream surfaces from the end-wall contours by the end-wall boundary layer displacement thicknesses described in Chapter 8. In that case, the lower limit of integration in Eq. (7-54) will be y_h rather than zero. That added sophistication has not resulted in any observable improvement to performance prediction accuracy, yet it can often complicate convergence and numerical stability. In either case, the interior stream surfaces are to be repositioned to yield the correct fraction of the mass flow calculated for the shroud stream surface using Eq. (7-54). The actual mass flow is not used so as to avoid any influence from numerical errors in conservation of mass or boundary layer analysis. Both of these numerical calculations are governed by specified convergence tolerances, but neither will yield an exact result. The correct locations of the interior stream surfaces for the computed flow field can be obtained by interpolation from this function to yield the values of y that correspond to the correct fraction of the mass flow function at y_s. These computed values of y yield the stream surface coordinates (z, r) for all stream surfaces on all quasi-normals.

$$z(y) = z_h + (z_s - z_h)(y - y_h)/(y_s - y_h) \tag{7-55}$$

$$r(y) = r_h + (r_s - r_h)(y - y_h)/(y_s - y_h) \tag{7-56}$$

These equations are written in general form, but are simplified in this writer's approach, where $y_h = 0$. If the stream surfaces are simply repositioned to these new positions, the streamline curvature numerical technique is known to be numerically unstable. Normal practice is to reposition the stream surfaces to locations that are some fraction, F, of the distance between the old positions and the new positions calculated for the current flow field data. This writer uses the numerical damping procedure suggested by Novak (1973). For quasi-normals outside of the blade passages, such as the present application, Novak recommends

$$\frac{1}{F} = 1 + \frac{(1 - M_m^2) y_s^2}{B^* (\Delta m)^2} \tag{7-57}$$

B^* is an empirical constant, typically about 8, and Δm is the minimum meridional spacing with the adjacent quasi-normals. When applying Eq. (7-57), this writer imposes the constraint that $M_m \leq 0.95$. Once the stream surfaces have been repositioned, new meridional coordinates are computed for all stream surfaces.

$$m = \int_{z_1}^{z} \left[1 + \left(\frac{\partial r}{\partial z} \right)^2 \right] dz \tag{7-58}$$

where the partial derivative in Eq. (7-58) is evaluated numerically from the stream surface (z, r) coordinates and z_1 is the value of z at the first quasi-normal. Other stream surface geometry data follow directly from Eqs. (7-1), (7-2), (7-3) and (7-9). Equation (7-58) sets $m = 0$ at the first quasi-normal, but that is arbitrary, since only relative values of m along a stream surface are significant for the present solution procedure.

7.5 FULL NORMAL EQUILIBRIUM SOLUTION

There are several useful solution procedures that can be applied for a through-flow analysis. The most general method is to solve the complete normal momentum equation as given in Eqs. (7-12) and (7-14). From the common practice of using radial lines as quasi-normals, this is often referred to as a full radial equilibrium solution. In the more general form used in this chapter, full normal equilibrium solution is a more appropriate term. Figure 7-3 shows a flow chart of a typical full normal-equilibrium solution procedure referenced to the methods outlined in Sections 7.2 through 7.4. The process starts by initializing the stream surfaces throughout the solution domain. This is usually accomplished by applying Eqs. (7-54) through (7-56), while assuming that the flow is uniform from the hub to the shroud and $\varepsilon = 0$. The inlet boundary conditions are imposed, and the flow is computed for the first quasi-normal using the iterative procedure described in Section 7.2. The process then involves solving of the flow field at all other quasi-normals. In this case, it is necessary to impose the linking calculations of Section 7.3 as well as the iterative procedure of Section 7.2. In

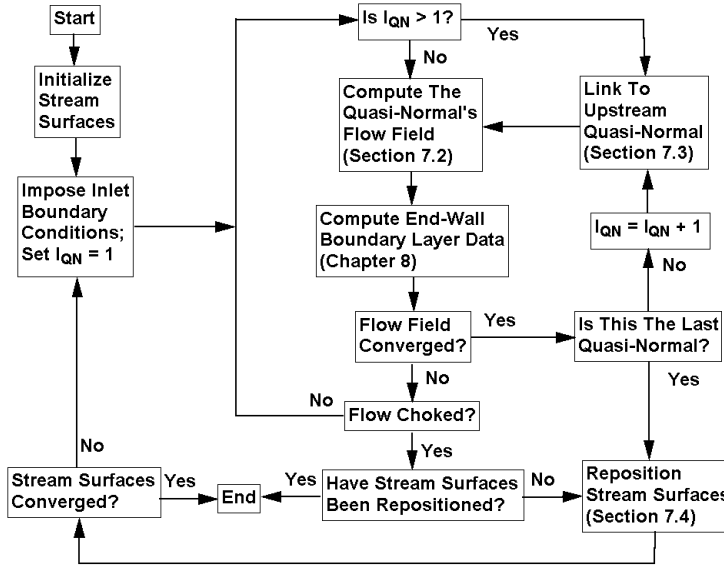

FIGURE 7-3 Full Normal Equilibrium Solution Flow Chart

general, the linking calculations depend on the flow field being calculated, so a second iteration loop is needed to converge on those calculations. When flow field on all quasi-normals has been treated, the stream surfaces can be repositioned using the procedures of Section 7.4. This requires a third or outer iteration loop to converge on the stream surface positions. When the flow field, linking calculations and stream surface positions are all self-consistent within an acceptable tolerance, the through-flow solution is complete. As shown in the flow chart, the end-wall boundary layer calculations described in Chapter 8 are normally carried out during this process, to include the end-wall boundary layer blockage effect.

The procedure is quite simple in concept, but a number of complications may be encountered. One common problem is that the flow is choked at a quasi-normal. It is not immediately obvious whether the choke condition is real, since incorrect stream surface positions might cause a false choke indication. The flow chart shows logic to require at least one completed stream surface reposition operation before the choke is considered valid. It may be desirable to require more than one completed reposition option. When the through-flow analysis is conducted interactively on personal computers, the simplest approach is to switch from an automatic iteration procedure to a manual one when choke occurs, such that the user can decide whether to continue for another outer iteration or terminate the solution. Another common complication is convergence problems with the outer iteration loop on stream surface positions. The damping procedure described in Section 7.4 is quite effective, but there is some uncertainty with regard to B^* in Eq. (7-57). $B^* = 8$ is a good choice for most problems,

but exceptions do occur. It is good practice to monitor the maximum stream surface position errors on successive iterations. If that error is increasing, B^* can be decreased to impose more damping on the numerical analysis. A good way to make this adjustment is to impose the following correction:

$$B^* \rightarrow (B^* + 1)/2 \tag{7-59}$$

7.6 SIMPLIFIED FORMS OF THE THROUGH-FLOW ANALYSIS

The full normal equilibrium through-flow analysis outlined in the previous sections is commonly referred to as the streamline curvature technique. It is well-suited for implementation in a relatively robust and reliable numerical analysis. But the streamline curvature technique is by no means totally free of numerical stability and convergence problems. The process of repositioning stream surfaces is, by far, the major source of these problems. It is also the process responsible for most of the computer time required for a through-flow analysis. The main purpose served by this relatively complex process is to determine ϕ, κ_m and ε. If these terms are neglected or approximated in some fashion, the entire outer iteration loop of the streamline curvature technique can be eliminated. The solution then becomes a simple marching solution, where the analysis proceeds through the solution domain, treating the quasi-normals in sequence. This is possible because the flow analysis on a quasi-normal becomes totally independent of conditions on downstream quasi-normals. The locations of the interior stream surfaces must still be established using Eqs. (7-54) through (7-56), but now the process is numerically stable and requires no numerical damping procedures. The process of relocating the stream surfaces can then be accomplished as a normal part of the process of solution at each quasi-normal.

In principle, this can be accomplished by solving Eqs. (7-2) and (7-9) using upstream finite-difference approximations. However, this really provides an estimate of the stream surface curvature within the blade passage rather than at the blade passage exit where the solution is to be accomplished. It is not at all uncommon for the stream surface curvature to be dramatically different at these two locations, often even having opposite signs. The difficulty arises from the fact that Eq. (7-9) is really equivalent to determining the second derivative of r as a function of z along the stream surface. Upstream finite-difference approximations to second derivatives are often seriously in error. At best, this approach may be capable of accounting for large curvature effects associated with passages having large end-wall contour curvatures. But in the majority of situations encountered in axial-flow compressors, it is better to ignore stream surface curvature entirely than to use upstream finite-difference approximations.

There certainly is merit to providing a through-flow analysis with the capability to approximate large stream surface curvatures present when passage curvatures are large. The inlet portion of the flow passage illustrated in Fig. 7-1 is a good example of a situation where stream surface curvature cannot be ignored. Since the end-wall contours are normally completely specified in advance, the

hub-and-shroud stream surface curvatures can be accurately estimated. A good way to extend a simplified through-flow analysis for it to be applicable to problems having significant passage curvature effects, is to assume that ϕ and κ_m vary linearly with y from the hub to the shroud. This approach can recognize significant passage-induced stream surface curvatures without the risk of producing the highly erroneous curvatures that can follow from an upstream finite-difference approach. In the context of axial-flow compressor performance analysis, performance predictions using this simplified model and the full normal equilibrium model are consistently found to be virtually identical. And the computer time required for solution is dramatically reduced when the simplified model is used.

The situation is quite different when a through-flow analysis is used as part of an aerodynamic design procedure. In these cases, typical practice is to specify one of the end-wall contours and to calculate the other from conservation of mass. This process of sizing the annulus may also include design of the blade rows, or it may employ a standard stage design. In either case, the slopes and curvatures of one of the end-walls cannot be well approximated in a marching type solution. In these cases, it is best to simply neglect stream surface curvature effects entirely. Since design-mode applications are normally restricted to stations before and after blade rows, this is generally a reasonable approximation. Usually any fine-tuning of the design that may be required is easily accomplished with a normal performance analysis. To apply this approximation to the through-flow analysis procedure outlined in the previous sections, it is only necessary to set $\varepsilon = \kappa_m = 0$ in Eqs. (7-12) through (7-19). This type of analysis has commonly been called a simple non-isentropic radial equilibrium solution, although in the more general quasi-normal structure used here, it is better described as a simple non-isentropic normal equilibrium solution.

There are also applications where the through-flow analysis must be further simplified by ignoring the entropy gradients along the quasi-normal. This occurs in industrial axial-flow compressors when designing a standard stage to be used throughout the compressor. This is often done as a means of minimizing the cost of manufacturing the compressor. Typically, the stagger angles of the blades in this standard stage will be adjusted somewhat through the machine to fine-tune the performance to the customer's requirements. Since the standard stage may be used in a variety of applications, it is not possible to compute the blade row performance in any general context. Nor do entropy gradient effects have much significance in this case, since they depend on all of the blade rows preceding the location of a specific stage. In this case, it is best to simply ignore entropy gradients as well as the curvature effects. This type of analysis is commonly referred to as a simple radial equilibrium solution. The term simple normal equilibrium is perhaps more appropriate, although generally this type of analysis will employ radial quasi-normals in any case.

Figure 7-4 illustrates a typical flow chart for any of these simplified forms of the through-flow analysis. On comparing this flow chart with the one shown in Fig. 7-3, it is seen that the entire outer iteration loop has been eliminated. In this case, repositioning of stream surfaces will be accomplished while computing the flow field at each quasi-normal. The procedure of Section 7.4 is used for this purpose, but without any numerical damping. This type of analysis is extremely fast

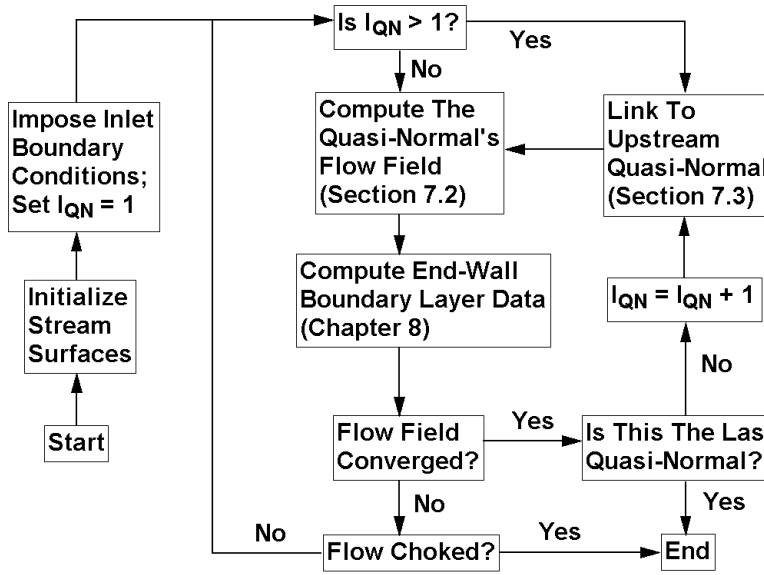

FIGURE 7-4 Simplified Through-Flow Analysis Flow Chart

and numerically very stable. The full normal equilibrium model certainly should be included for generality. But it is truly remarkable how seldom it is really required for typical axial-flow compressor applications. In addition, the simplified forms allow application of the through-flow analysis to a number of aerodynamic design functions where use of the full normal equilibrium model would be totally impractical.

In summary, a through-flow analysis should normally be developed in a fairly general form to include the capability of employing any of the following aerodynamic models.

- Full normal equilibrium.
- Approximate (linear, hub to shroud) stream surface slope and curvature.
- Simple non-isentropic normal equilibrium.
- Simple (isentropic) normal equilibrium.

In this way, the same through-flow analysis can be applied to a variety of axial-flow compressor aerodynamic design and analysis functions.

7.7 ANNULUS SIZING

The annulus sizing process mentioned in the previous section is one useful aerodynamic design function that is conveniently incorporated directly into the

through-flow analysis. In this mode of solution, only one of the end-wall contours is specified. The analysis is used to determine the other end-wall contour, while conserving mass and matching a desired distribution of W_m through the compressor. Typically, the W_m distribution is specified for the mean stream surface, although any other stream surface can be used as well. For generality, a superscript, *, will be used to designate parameters on the stream surface for which W_m will be specified. The special requirements for annulus sizing include

- Specify z and r for one end-wall contour and the angle, λ, of Fig. 7-2 for all quasi-normals.
- Specify values of W_m for the selected stream surface for all quasi-normals.
- Neglect stream surface curvature effects, typically using the simple nonisentropic normal equilibrium model.

The annulus area, A, at any quasi-normal is given by

$$A = \pi(r_s + r_h)y_s \tag{7-60}$$

As an initial estimate for the annulus area, use the specified meridional velocity, the total density and conservation of mass

$$A = \dot{m} / (\rho_t^* W_m^*) \tag{7-61}$$

where the inlet total density is used for the first quasi-normal, and its value at the upstream quasi-normal is used for all others. From Eq. (7-60) and the specified value of λ, it is easily shown that

$$r_s^2 = r_h^2 + (A\cos\lambda)/\pi \tag{7-62}$$

$$y_s = A / [\pi(r_s + r_h)] \tag{7-63}$$

$$z_s = z_h - y_s \sin\lambda \tag{7-64}$$

Equations (7-62) through (7-64) yield the coordinates of the unknown end-wall contour from those of the known contour and the passage area. Next, the usual through-flow analysis is conducted while using the specified meridional velocity as a constant of integration in Eq. (7-35). Although Eq. (7-35) is written with the hub meridional velocity (at $y = 0$) as the constant of integration, the value at y^* can be used with a simple substitution. From Eq. (7-35) it is easily shown that

$$W_m(0) = W_m^* / F(y^*) - \int_0^{y^*} \frac{f_4(y)}{F(y)} dy \tag{7-65}$$

The annulus sizing differs from the procedures presented for the analysis mode only with regard to the application of Eq. (7-5). Here, it is used to compute the

mass flow rate, $\dot{m}_c$, for the estimated annulus area. Then the annulus area estimate is improved by

$$A \rightarrow A\dot{m} / \dot{m}_c \tag{7-66}$$

and the process is repeated until acceptable convergence on the mass flow rate is achieved.

7.8 NUMERICAL APPROXIMATIONS

A numerical analysis based on the procedures described in this chapter is relatively straightforward, except as it relates to approximations for the stream surface curvature terms. When the streamline curvature technique was introduced, common practice was to employ spline-connected cubic approximations for this purpose (e.g, see Walsh et al., 1962). Although the spline fit seems almost ideal for the smooth curves expected, experience eventually convinced most investigators that it is not a particularly good choice. The spline fit has a definite tendency to destabilize the analysis, to increase the demands on the numerical damping procedures.

The simple three-point finite-difference approximation for the partial derivatives in Eqs. (7-2) and (7-9) is a much better choice for this application. These are derived from truncated Taylor series approximations for the central point in a series of three points, similar to the derivation of Eqs. (5-35) and (5-36). In the present case, the points are not likely to have equally spacing, as was the case in Chapter 5. A more general approximation can be shown to be

$$\left[\frac{\partial f}{\partial m}\right]_2 = \frac{1}{m_3 - m_1}\left[\frac{(m_3 - m_2)(f_2 - f_1)}{m_2 - m_1} + \frac{(m_2 - m_1)(f_3 - f_2)}{m_3 - m_2}\right] \tag{7-67}$$

where the subscripts 1, 2 and 3 designate any three successive points along the curve. Similarly, three-point difference approximations can also be derived for end points on the curve to yield

$$\left[\frac{\partial f}{\partial m}\right]_1 = \frac{1}{m_3 - m_2}\left[\frac{(m_3 - m_1)(f_2 - f_1)}{m_2 - m_1} - \frac{(m_2 - m_1)(f_3 - f_1)}{m_3 - m_1}\right] \tag{7-68}$$

$$\left[\frac{\partial f}{\partial m}\right]_3 = \frac{1}{m_2 - m_1}\left[\frac{(m_3 - m_1)(f_3 - f_2)}{m_3 - m_2} - \frac{(m_3 - m_2)(f_3 - f_1)}{m_3 - m_1}\right] \tag{7-69}$$

For this application, which can often induce numerical stability problems, a simple two-point difference approximation is a better choice for end points, i.e.,

$$\left[\frac{\partial f}{\partial m}\right]_1 = \left[\frac{\partial f}{\partial m}\right]_2 = \frac{f_2 - f_1}{m_2 - m_1} \tag{7-70}$$

Equation (7-70) will also be required for all quasi-normals when the simplified through-flow models of Section 7.6, since data at $m = m_3$ will not be known when solving at $m = m_2$, in those simple marching type analyses.

Solution of Eq. (7-35) requires numerical approximations for partial derivatives with respect to y and for integrals with respect to y. Equations (7-67) through (7-69) have been found to be good choices for the derivative approximations at interior and end points, where y is substituted for m. For numerical integration, an approximation for the second derivative at interior values of y is also required. A suitable three-point approximation can be derived from truncated Taylor series to yield

$$\left[\frac{\partial^2 f}{\partial y^2}\right]_2 = \frac{2}{y_3 - y_1}\left[\frac{f_3 - f_2}{y_3 - y_2} - \frac{f_2 - f_1}{y_2 - y_1}\right] \tag{7-71}$$

A Taylor series approximation to the integral between points 1 and 2, where point 2 is an interior point, is easily shown to be

$$\int_{y_1}^{y_2} f(y)dy = \left(f(y_2) - \left[\frac{\partial f}{\partial y}\right]_2 \frac{(y_2 - y_1)}{2} + \left[\frac{\partial^2 f}{\partial y^2}\right]_2 \frac{(y_2 - y_1)^2}{6}\right)(y_2 - y_1) \tag{7-72}$$

Similarly, the integral between points 2 and 3, where point 3 is the last point, is given by

$$\int_{y_2}^{y_3} f(y)dy = \left(f(y_2) + \left[\frac{\partial f}{\partial y}\right]_2 \frac{(y_3 - y_2)}{2} + \left[\frac{\partial^2 f}{\partial y^2}\right]_2 \frac{(y_3 - y_2)^2}{6}\right)(y_3 - y_2) \tag{7-73}$$

These two equations can be used to compute all integrals with respect to y from 0 to y_s for any number of stream surfaces by simple summation of results between successive points. Equations (7-67) and (7-71) provide the approximations for the derivative terms in Eqs. (7-72) and (7-73).

EXERCISES

7.1 Geometry data for an axial-flow compressor blade is normally specified as a function of radius. Data sufficient to define the blade might include the chord, c, the thickness-to-chord ratio, t_b / c, and any two of the following: camber angle, θ, stagger angle, γ, inlet angle, κ_1, or exit angle, κ_2. The number of blades, Z, and the location of maximum camber, a/c, will be constant for each blade row. A through-flow analysis is to be applied in an aerodynamic performance analysis such that the blade geometry on each stream surface is required so that the empirical models of Chapter 6 can be used to

estimate the blade row loss and fluid turning. Consider a stream surface passing through a blade row with inlet coordinates (z_1, r_1) and exit coordinates (z_2, r_2). Develop a method to estimate the blade geometry on the stream surface from the known blade geometry as a function of radius.

7.2 Equation (7-29) is recommended for evaluating the meridional gradient of the meridional velocity component. Alternatively, this gradient might be evaluated using the finite-difference approximations of Section 7.8. Discuss the relative merits of these two alternative approximations.

7.3 Equation (7-39) has been recommended as an approximate criterion for choked flow in the annular passage, outside of the blade rows. A rigorous calculation of the choked flow limit could be accomplished by determining the constant of integration, $W_m(0)$, for Eq. (7-35) that yields the maximum mass flow rate. Give two reasons why the approximate criterion should be adequate for a through-flow analysis in an axial-flow compressor. Under what conditions might the more rigorous method be preferred?

7.4 Discuss the advantages and disadvantages of using Eqs. (7-31) through (7-33) as a means of avoiding a singularity in Eq. (7-34). Consider the accuracy of the approximation used for both interior and end-wall stream surfaces. For a fully converged inviscid through-flow solution, where can such a singularity occur? Is the approximation more acceptable if an end-wall boundary layer analysis is conducted as part of the overall solution?